

A Search for Electron Neutrino Appearance at the $\Delta m^2 \sim 1 \text{ eV}^2$ Scale

A. A. Aguilar-Arevalo⁵, A. O. Bazarko¹², S. J. Brice⁷, B. C. Brown⁷, L. Bugel⁵, J. Cao¹¹, L. Coney⁵, J. M. Conrad⁵, D. C. Cox⁸, A. Curioni¹⁶, Z. Djurcic⁵, D. A. Finley⁷, B. T. Fleming¹⁶, R. Ford⁷, F. G. Garcia⁷, G. T. Garvey⁹, C. Green^{7,9}, J. A. Green^{8,9}, T. L. Hart⁴, E. Hawker¹⁵, R. Imlay¹⁰, R. A. Johnson³, P. Kasper⁷, T. Katori⁸, T. Kobilarcik⁷, I. Kourbanis⁷, S. Koutsoliotas², E. M. Laird¹², J. M. Link¹⁴, Y. Liu¹¹, Y. Liu¹, W. C. Louis⁹, K. B. M. Mahn⁵, W. Marsh⁷, P. S. Martin⁷, G. McGregor⁹, W. Metcalf¹⁰, P. D. Meyers¹², F. Mills⁷, G. B. Mills⁹, J. Monroe⁵, C. D. Moore⁷, R. H. Nelson⁴, P. Nienaber¹³, S. Ouedraogo¹⁰, R. B. Patterson¹², D. Perevalov¹, C. C. Polly⁸, E. Prebys⁷, J. L. Raaf³, H. Ray⁹, B. P. Roe¹¹, A. D. Russell⁷, V. Sandberg⁹, R. Schirato⁹, D. Schmitz⁵, M. H. Shaevitz⁵, F. C. Shoemaker¹², D. Smith⁶, M. Sorel⁵, P. Spentzouris⁷, I. Stancu¹, R. J. Stefanski⁷, M. Sung¹⁰, H. A. Tanaka¹², R. Tayloe⁸, M. Tzanov⁴, R. Van de Water⁹, M. O. Wascko¹⁰, D. H. White⁹, M. J. Wilking⁴, H. J. Yang¹¹, G. P. Zeller⁵, E. D. Zimmerman⁴

(The MiniBooNE Collaboration)

¹University of Alabama; Tuscaloosa, AL 35487

²Bucknell University; Lewisburg, PA 17837

³University of Cincinnati; Cincinnati, OH 45221

⁴University of Colorado; Boulder, CO 80309

⁵Columbia University; New York, NY 10027

⁶Embry Riddle Aeronautical University; Prescott, AZ 86301

⁷Fermi National Accelerator Laboratory; Batavia, IL 60510

⁸Indiana University; Bloomington, IN 47405

⁹Los Alamos National Laboratory; Los Alamos, NM 87545

¹⁰Louisiana State University; Baton Rouge, LA 70803

¹¹University of Michigan; Ann Arbor, MI 48109

¹²Princeton University; Princeton, NJ 08544

¹³Saint Mary's University of Minnesota; Winona, MN 55987

¹⁴Virginia Polytechnic Institute & State University; Blacksburg, VA 24061

¹⁵Western Illinois University; Macomb, IL 61455

¹⁶Yale University; New Haven, CT 06520

(Dated: November 26, 2024)

The MiniBooNE Collaboration reports first results of a search for ν_e appearance in a ν_μ beam. With two largely independent analyses, we observe no significant excess of events above background for reconstructed neutrino energies above 475 MeV. The data are consistent with no oscillations within a two-neutrino appearance-only oscillation model.

This Letter reports the initial results from a search for $\nu_\mu \rightarrow \nu_e$ oscillations by the MiniBooNE Collaboration. MiniBooNE was motivated by the result from the Liquid Scintillator Neutrino Detector (LSND) experiment [1], which has presented evidence for $\bar{\nu}_\mu \rightarrow \bar{\nu}_e$ oscillations at the $\Delta m^2 \sim 1 \text{ eV}^2$ scale. Although the Karlsruhe Rutherford Medium Energy Neutrino Experiment (KARMEN) observed no evidence for neutrino oscillations [2], a joint analysis [3] showed compatibility at 64% CL. Evidence for neutrino oscillations also comes from solar-neutrino [4, 5, 6, 7, 8] and reactor-antineutrino experiments [9], which have observed ν_e disappearance at $\Delta m^2 \sim 8 \times 10^{-5} \text{ eV}^2$, and atmospheric-neutrino [10, 11, 12, 13] and long-baseline accelerator-neutrino experiments [14, 15], which have observed ν_μ disappearance at $\Delta m^2 \sim 3 \times 10^{-3} \text{ eV}^2$.

If all three phenomena are caused by neutrino oscillations, these three Δm^2 scales cannot be accommodated in an extension of the Standard Model that allows only three neutrino mass eigenstates. An explanation of all three mass scales with neutrino oscillations requires the

addition of one or more sterile neutrinos [16] or further extensions of the Standard Model (*e.g.*, [17]).

The analysis of the MiniBooNE neutrino data presented here is performed within a two neutrino appearance-only $\nu_\mu \rightarrow \nu_e$ oscillation model which uses ν_μ events to constrain the predicted ν_e rate. Other than oscillations between these two species, we assume no effects beyond the Standard Model.

The experiment uses the Fermilab Booster neutrino beam, which is produced from 8 GeV protons incident on a 71-cm-long by 1-cm-diameter beryllium target. The proton beam typically has 4×10^{12} protons per $\sim 1.6 \mu\text{s}$ beam spill at a rate of 4 Hz. The number of protons on target per spill is measured by two toroids in the beamline. The target is located inside a focusing horn, which produces a toroidal magnetic field that is pulsed in time with the beam at a peak current of 174 kA. Positively charged pions and kaons, focused by the horn, pass through a 60-cm-diameter collimator and can decay in a 50-m-long tunnel, which is 91 cm in radius and filled with

air at atmospheric pressure.

The center of the detector is 541 m from the front of the beryllium target and 1.9 m above the center of the neutrino beam. There is about 3 m of dirt overburden above the detector, which is a spherical tank of inner radius 610 cm filled with 800 tons of pure mineral oil (CH_2) with a density of 0.86 g/cm^3 and an index of refraction of 1.47. The light attenuation length in the mineral oil increases with wavelength from a few cm at 280 nm to over 20 m at 400 nm. Charged particles passing through the oil can emit both directional Cherenkov light and isotropic scintillation light. An optical barrier separates the detector into two regions, an inner volume with a radius of 575 cm and an outer volume 35 cm thick. The optical barrier supports 1280 equally-spaced inward-facing 8-inch photomultiplier tubes (PMTs), providing 10% photocathode coverage. An additional 240 tubes are mounted in the outer volume, which acts as a veto shield, detecting particles entering or leaving the detector. Two types of PMT are used: 1198 Hamamatsu model R1408 with 9 stages and 322 Hamamatsu model R5912 with 10 stages. Approximately 98% of the PMTs have worked well throughout the data taking period.

The experiment triggers on every beam spill, with all PMT hits recorded for a $19.2 \mu\text{s}$ window beginning $4.4 \mu\text{s}$ before the spill. Other triggers include a random trigger for beam-unrelated measurements, a laser-calibration trigger, cosmic-muon triggers, and a trigger to record neutrino-induced events from the nearby Neutrinos at the Main Injector (NuMI) beamline [18]. The detector electronics, refurbished from LSND [19], digitize the times and integrated charges of PMT hits. PMT hit thresholds are ~ 0.1 photoelectrons (PE); the single-PE time resolutions achieved by this system are $\sim 1.7 \text{ ns}$ and $\sim 1.2 \text{ ns}$ for the two types of PMTs. One PE corresponds to $\sim 0.2 \text{ MeV}$ of electron energy. Laser calibration, consisting of optical fibers that run from the laser to dispersion flasks inside the tank, is run continuously at 3.33 Hz to determine PMT gains and time offsets. Averaged over the entire run, the beam-on livetime of the experiment is greater than 98%.

The ν_μ energy spectrum peaks at 700 MeV and extends to approximately 3000 MeV. Integrated over the neutrino flux, interactions in MiniBooNE are mostly charged-current quasi-elastic (CCQE) scattering (39%), neutral-current (NC) elastic scattering (16%), charged-current (CC) single pion production (29%), and NC single pion production (12%). Multi-pion and deep-inelastic scattering contributions are $< 5\%$. NC elastic scattering, with only a recoil nucleon and a neutrino in the final state, typically produces relatively little light in the detector and contributes only 3 events to the final background estimate.

Table I shows the estimated number of events with reconstructed neutrino energy, E_ν^{QE} , between 475 MeV and 1250 MeV after the complete event selection from

TABLE I: *The estimated number of events with systematic error in the $475 < E_\nu^{QE} < 1250 \text{ MeV}$ energy range from all of the significant backgrounds, together with the estimated number of signal events for $0.26\% \nu_\mu \rightarrow \nu_e$ transmutation, after the complete event selection.*

Process	Number of Events
ν_μ CCQE	10 ± 2
$\nu_\mu e \rightarrow \nu_\mu e$	7 ± 2
Miscellaneous ν_μ Events	13 ± 5
NC π^0	62 ± 10
NC $\Delta \rightarrow N\gamma$	20 ± 4
NC Coherent & Radiative γ	< 1
Dirt Events	17 ± 3
ν_e from μ Decay	132 ± 10
ν_e from K^+ Decay	71 ± 26
ν_e from K_L^0 Decay	23 ± 7
ν_e from π Decay	3 ± 1
Total Background	358 ± 35
$0.26\% \nu_\mu \rightarrow \nu_e$	163 ± 21

all of the significant backgrounds, where E_ν^{QE} is determined from the reconstructed lepton energy and angle with respect to the known neutrino direction. The background estimate includes antineutrino events, which represent $< 2\%$ of the total. Also shown is the estimated number of ν_e CCQE signal events for the LSND central expectation of $0.26\% \nu_\mu \rightarrow \nu_e$ transmutation. Studies of random triggers have established that no significant backgrounds survive the analysis cuts other than those due to beam related neutrinos, which can be divided into either ν_μ -induced or ν_e -induced backgrounds. The small fraction of ν_e from μ , K , and π decay in the beamline gives a background that is indistinguishable from oscillations except for the energy spectrum. CC ν_μ events are distinguished from ν_e events by the distinct patterns of Cherenkov and scintillation light for muons and electrons, as well as by the observation of a delayed electron from the muon decay, which is observed $> 80\%$ of the time from ν_μ CCQE events. NC π^0 events with only a single electromagnetic shower reconstructed are the main ν_μ -induced background, followed by radiative Δ decays giving a single photon, and then neutrino interactions in the dirt surrounding the detector, which can mimic a signal if a single photon, mostly from π^0 decay, penetrates the veto and converts in the fiducial volume.

We use PMT charge and time information in the $19.2 \mu\text{s}$ window to reconstruct neutrino interactions and identify the product particles. This time window is defined as an “event” and is divided into “subevents”, collections of PMT hits clustered in time within $\sim 100 \text{ ns}$. A ν_μ CCQE event with a muon stopping within the tank may have two subevents: the first subevent from particles produced at the neutrino interaction, the second from the muon decay to an electron. A ν_e CCQE event has a single subevent.

To ensure stable, well-targeted beam at full horn current, it is required that the two monitoring toroids agree to within 5%, the estimated transverse containment of the beam in the target be greater than 95%, and the measured horn current be within 3% of its nominal value. The event time at the detector must be consistent with the beam delivery time (both determined by GPS), and the event must pass a number of data integrity checks. The beam quality requirements reject 0.7% of the events, while the detector time and quality requirements remove a further 1.8%, with the remaining data corresponding to $(5.58 \pm 0.12) \times 10^{20}$ protons on target.

Next, events with exactly one subevent (as expected for ν_e CCQE events) are selected. By requiring that the subevent have fewer than 6 hits in the veto and more than 200 hits in the main tank (above the muon-decay electron endpoint), entering cosmic-ray muons and their associated decay electrons are eliminated. The average time of hits in the subevent is required to be within the beam time window of 4-7 μ s. These cuts yield a cosmic ray rejection of greater than 1000:1.

After these initial cuts, the surviving events are reconstructed under four hypotheses: a single electron-like Cherenkov ring, a single muon-like ring, two photon-like rings with unconstrained kinematics, and two photon-like rings with $M_{\gamma\gamma} = m_{\pi^0}$ (see Fig. 1). Photon-like rings are assumed to be identical to electrons, but allowed to be independently displaced from the neutrino interaction vertex. The reconstruction uses a detailed model of extended-track light production and propagation in the tank to predict the charge and time of hits on each PMT. Event parameters are varied to maximize the likelihood of the observed hits, yielding the vertex position and time of the event and the direction, energy, and, for photons, the conversion distance of the ring(s). For ν_e events, the event vertex, direction, and energy are reconstructed on average with resolutions of 22 cm, 2.8°, and 11%, respectively, while NC π^0 events are reconstructed with a π^0 mass resolution of 20 MeV/ c^2 .

The final analysis cuts were designed to isolate a sample of ν_e -induced events that were primarily CCQE. The only data that were used in developing the analysis were samples that Monte Carlo (MC) simulation had indicated could not contain a significant number of $\nu_\mu \rightarrow \nu_e$ oscillation events. We require that the electron-hypothesis event vertex and muon-hypothesis track endpoint occur at radii < 500 cm and < 488 cm, respectively, to ensure good event reconstruction and efficiency for possible muon decay electrons. We require visible energy $E_{vis} > 140$ MeV. We then apply particle identification (PID) cuts to reject muon and π^0 events. These are E_{vis} -dependent cuts on $\log(L_e/L_\mu)$, $\log(L_e/L_{\pi^0})$, and $M_{\gamma\gamma}$, where L_e , L_μ , and L_{π^0} are the likelihoods for each event maximized under the electron 1-ring, muon 1-ring, and fixed-mass 2-ring fits, and $M_{\gamma\gamma}$ is from the unconstrained two-ring fit. These also enhance the fraction of CCQE

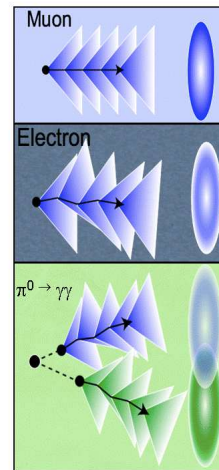


FIG. 1: Events in MiniBooNE are reconstructed as either a muon event, an electron event, or a π^0 event.

TABLE II: *The observed number of ν_e CCQE candidate events and the efficiency for $\nu_\mu \rightarrow \nu_e$ CCQE oscillation events after each cut is applied sequentially.*

Selection	#Events	ν_e CCQE Efficiency
Cosmic Ray Cuts	109,590	100%
Fiducial Volume Cuts	68,143	$55.2 \pm 1.9\%$
PID Cuts	2037	$30.6 \pm 1.4\%$
$475 < E_\nu^{QE} < 1250$ MeV	380	$20.3 \pm 0.9\%$

events among the surviving electron candidates. Table II shows the observed number of ν_e CCQE candidate events and the efficiency for $\nu_\mu \rightarrow \nu_e$ CCQE oscillation events after each cut is applied sequentially. A total of 380 data events remains after the complete selection.

Detailed Monte Carlo simulations of the beam and detector were used to make initial estimates of the flux and detector efficiencies. The Booster neutrino beam flux at the detector is modeled using a GEANT4-based simulation [20] of the beamline geometry. Pion and kaon production in the target is parametrized [21] based on a global fit to proton-beryllium particle production data [22]. The kaon flux has been cross-checked with high-energy events above 1250 MeV and with an off-axis muon spectrometer that viewed the secondary beamline from an angle of 7°. This detector determined the flux of muons with high transverse momentum, which originate mostly from kaon decays, to be consistent with the MC predictions.

The v3 NUANCE [23] event generator simulates neutrino interactions in mineral oil. Modifications are made to NUANCE which include adjustment of the axial form factor of the nucleon for quasi-elastic scattering, the Pauli blocking model, and coherent pion production cross sections based on fits to MiniBooNE ν_μ data [24]. In addition, the final state interaction model has been tuned to

reproduce external pion-carbon rescattering data [25], an explicit model of nuclear de-excitation photon emission for carbon has been added [26], and the angular correlations for Δ decay are modified to be in accord with the model of Rein and Sehgal [27].

Particles from NUANCE-generated final states are propagated through a GEANT3-based simulation [28] of the detector, with the subsequent decays, strong, and electroweak interactions in the detector medium included. Most particular to MiniBooNE, the emission of optical and near-UV photons via Cherenkov radiation and scintillation is simulated, with each photon individually tracked, undergoing scattering, fluorescence, and reflection, until it is absorbed [29]. Small-sample measurements of transmission, fluorescence, and scattering are used in the model. Muon decay electrons are used to calibrate both the light propagation in the detector and the energy scale. The amount of scintillation light is constrained from NC elastic scattering events. The charge and time response of the electronics is simulated, and from this point onward, data and MC calculations are treated identically by the analysis programs.

All of the major ν_μ -induced backgrounds are constrained by our measurements outside the signal region. The inclusive CC background is verified by comparing data to MC calculations for events with two subevents, where the second subevent has < 200 tank hits and is consistent with a muon-decay electron. As the probability for μ^- capture in the oil is 8%, there are an order of magnitude more CC inclusive scattering events with two subevents than with only one subevent, so that this background is well checked. These data events are also modified by moving the hits of the second subevent earlier in time to model early, inseparable decays which can look more like an electron.

To determine the NC π^0 background, π^0 rates are measured in bins of momentum by counting events in the $\gamma\gamma$ mass peak. The MC simulation is used to correct the production rate for inefficiency, background and resolution (corrections are $\sim 10\%$). To match the data angular distribution, the π^0 candidates are fit to MC templates (in mass and angle) for resonant and coherent production (generated using the model of Rein and Sehgal [27]) as well as a template for non- π^0 background events. The fitted parameters are used to reweight π^0 from the MC calculations and to constrain the $\Delta \rightarrow N\gamma$ rate, which has a branching ratio at the peak of the Δ resonance of 0.56%. NC coherent γ background [30] and NC radiative γ background [31] are both estimated to be negligible. The background from interactions in the dirt surrounding the detector is measured from a sample of inward-pointing events inside the tank at high radius.

A sample of $\sim 10^5$ candidate ν_μ CCQE events is obtained by requiring a μ -decay electron with a reconstructed vertex consistent with the estimated endpoint of the parent muon's track (60% efficiency). The observed

rate of these ν_μ CCQE events is used to correct the MC predictions for ν_e signal events, ν_μ CC backgrounds, and ν_e from μ backgrounds (which share their π parentage with the ν_μ CCQE events). These constraints increase the event normalization by 32% and greatly reduce the rate uncertainties on these three components of the final analysis sample.

Systematic errors are associated with neutrino fluxes, the detector model, and neutrino cross sections. The neutrino flux systematic errors are determined from the uncertainties of particle production measurements, the detector model systematic errors are mostly determined from fits to MiniBooNE data, and the neutrino cross section systematic errors are determined from MiniBooNE data as well as from external sources, both experimental and theoretical. These groups of errors are taken to be independent, and, for each, an individual error matrix is formed that includes the full correlation among the systematic parameters. This is mapped to a matrix describing the correlated errors in predicted background plus possible signal in eight $\nu_e E_\nu^{QE}$ bins. The final covariance matrix for all sources of uncertainty (statistical and systematic) is the sum of the individual error matrices. The signal extraction is performed by computing the χ^2 comparing data to predicted background plus a $(\sin^2(2\theta), \Delta m^2)$ -determined contribution from $\nu_\mu \rightarrow \nu_e$ two-neutrino oscillations in the eight E_ν^{QE} bins and minimizing with respect to these two oscillation parameters across their physical range.

With the analysis cuts set, a signal-blind test of data-MC agreement in the signal region was performed. The full two-neutrino oscillation fit was done in the range $300 < E_\nu^{QE} < 3000$ MeV and, with no information on the fit parameters revealed, the sum of predicted background and simulated best-fit signal was compared to data in several variables, returning only the χ^2 . While agreement was good in most of the comparisons, the E_{vis} spectrum had a χ^2 probability of only 1%. This triggered further investigation of the backgrounds, focusing on the lowest energies where ν_μ -induced backgrounds, some of which are difficult to model, are large. As part of this study, one more piece of information from the signal region was released: unsigned bin-by-bin fractional discrepancies in the E_{vis} spectrum. While ambiguous, these reinforced suspicions about the low-energy region. Though we found no specific problems with the background estimates, it was found that raising the minimum E_ν^{QE} of the fit region to 475 MeV greatly reduced a number of backgrounds with little impact on the fit's sensitivity to oscillations. We thus performed our oscillation fits in the energy range $475 < E_\nu^{QE} < 3000$ MeV and opened the full data set.

The top plot of Fig. 2 shows candidate ν_e events as a function of E_ν^{QE} . The vertical dashed line indicates the minimum E_ν^{QE} used in the two-neutrino oscillation analysis. There is no significant excess of events ($22 \pm 19 \pm 35$

events) for $475 < E_\nu^{QE} < 1250$ MeV; however, an excess of events ($96 \pm 17 \pm 20$ events) is observed below 475 MeV. This low-energy excess cannot be explained by a two-neutrino oscillation model, and its source is under investigation. The dashed histogram in Fig. 2 shows the predicted spectrum when the best-fit two-neutrino oscillation signal is added to the predicted background. The bottom panel of the figure shows background-subtracted data with the best-fit two-neutrino oscillation and two oscillation points from the favored LSND region. The oscillation fit in the $475 < E_\nu^{QE} < 3000$ MeV energy range yields a χ^2 probability of 93% for the null hypothesis, and a probability of 99% for the ($\sin^2 2\theta = 10^{-3}$, $\Delta m^2 = 4 \text{ eV}^2$) best-fit point.

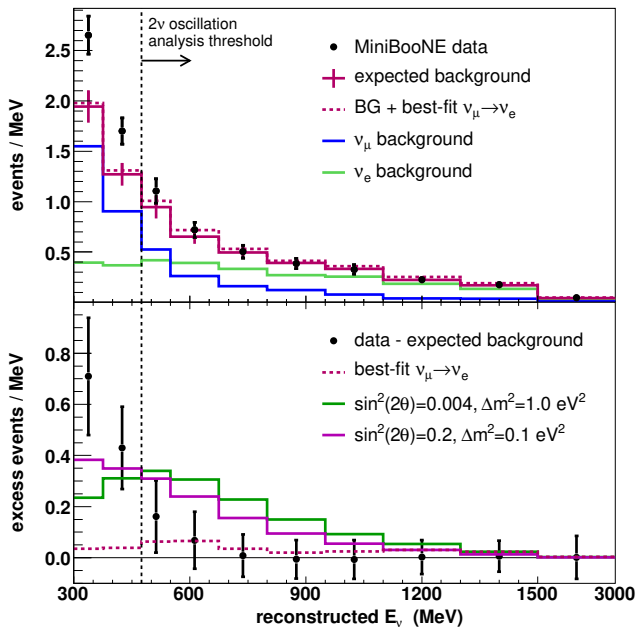


FIG. 2: The top plot shows the number of candidate ν_e events as a function of E_ν^{QE} . The points represent the data with statistical error, while the histogram is the expected background with systematic errors from all sources. The vertical dashed line indicates the threshold used in the two-neutrino oscillation analysis. Also shown are the best-fit oscillation spectrum (dashed histogram) and the background contributions from ν_μ and ν_e events. The bottom plot shows the number of events with the predicted background subtracted as a function of E_ν^{QE} , where the points represent the data with total errors and the two histograms correspond to LSND solutions at high and low Δm^2 .

A single-sided raster scan to a two neutrino appearance-only oscillation model is used in the energy range $475 < E_\nu^{QE} < 3000$ MeV to find the 90% CL limit corresponding to $\Delta\chi^2 = \chi_{limit}^2 - \chi_{bestfit}^2 = 1.64$. As shown by the top plot in Fig. 3, the LSND 90% CL allowed region is excluded at the 90% CL. A joint analysis as a function of Δm^2 , using a combined χ^2 of the best fit values and errors for LSND and MiniBooNE, excludes

at 98% CL two-neutrino appearance oscillations as an explanation of the LSND anomaly. The bottom plot of Fig. 3 shows limits from the KARMEN [2] and Bugey [32] experiments.

A second analysis developed simultaneously and with the same blindness criteria used a different set of reconstruction programs, PID algorithms, and fitting and normalization processes. The reconstruction used a simpler model of light emission and propagation. The PID used 172 quantities such as charge and time likelihoods in angular bins, $M_{\gamma\gamma}$, and likelihood ratios (electron/pion and electron/muon) as inputs to boosted decision tree algorithms [33] that are trained on sets of simulated signal events and background events with a cascade-training technique [34]. In order to achieve the maximum sensitivity to oscillations, the ν_μ -CCQE data sample with two subevents were fit simultaneously with the ν_e -CCQE candidate sample with one subevent. By forming a χ^2 using both data sets and using the corresponding covariance matrix to relate the contents of the bins of the two distributions, the errors in the oscillation parameters that best describe the ν_e -CCQE candidate data set were well constrained by the observed ν_μ -CCQE data. This procedure is partially equivalent to doing a ν_e to ν_μ ratio analysis where many of the systematic uncertainties cancel.

The two analyses are very complementary, with the second having a better signal-to-background ratio, but the first having less sensitivity to systematic errors from detector properties. These different strengths resulted in very similar oscillation sensitivities and, when unblinded, yielded the expected overlap of events and very similar oscillation fit results. The second analysis also sees more events than expected at low energy, but with less significance. Based on the predicted sensitivities before unblinding, we decided to present the first analysis as our oscillation result, with the second as a powerful cross-check.

In summary, while there is a presently unexplained discrepancy with data lying above background at low energy, there is excellent agreement between data and prediction in the oscillation analysis region. If the oscillations of neutrinos and antineutrinos are the same, this result excludes two neutrino appearance-only oscillations as an explanation of the LSND anomaly at 98% CL.

We acknowledge the support of Fermilab, the Department of Energy, and the National Science Foundation. We thank Los Alamos National Laboratory for LDRD funding. We acknowledge Bartoszek Engineering for the design of the focusing horn. We acknowledge Dmitri Toptygin, Anna Pla, and Hans-Otto Meyer for optical measurements of mineral oil. This research was done using resources provided by the Open Science Grid, which is supported by the NSF and DOE-SC. We also acknowledge the use of the LANL Pink cluster and Condor soft-

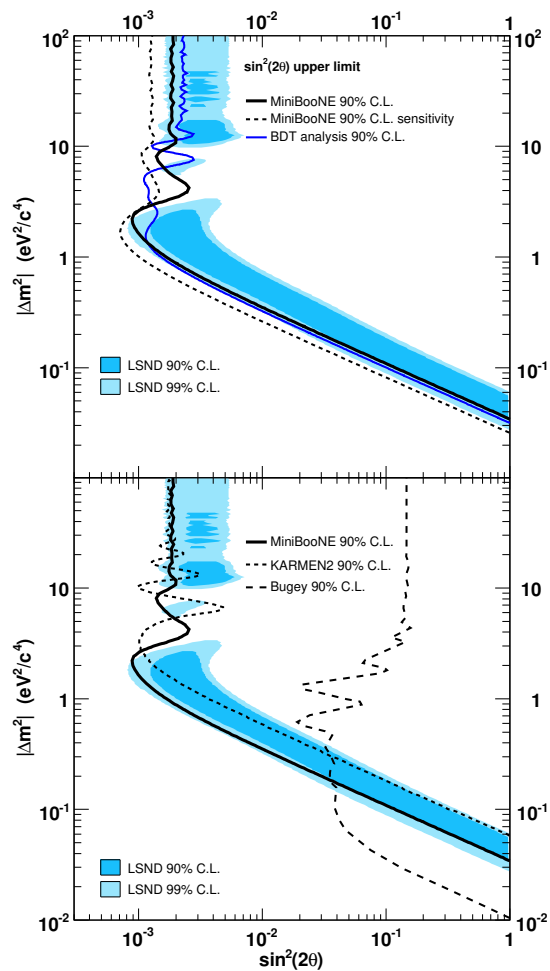


FIG. 3: The top plot shows the MiniBooNE 90% CL limit (thick solid curve) and sensitivity (dashed curve) for events with $475 < E_{\nu}^{QE} < 3000$ MeV within a two neutrino oscillation model. Also shown is the limit from the boosted decision tree analysis (thin solid curve) for events with $300 < E_{\nu}^{QE} < 3000$ MeV. The bottom plot shows the limits from the KARMEN [2] and Bugey [32] experiments. The MiniBooNE and Bugey curves are 1-sided upper limits on $\sin^2 2\theta$ corresponding to $\Delta\chi^2 = 1.64$, while the KARMEN curve is a “unified approach” 2D contour. The shaded areas show the 90% and 99% CL allowed regions from the LSND experiment.

ware in the analysis of the data.

-
- [1] C. Athanassopoulos *et al.*, Phys. Rev. Lett. 75, 2650 (1995); 77, 3082 (1996); 81, 1774 (1998); A. Aguilar *et al.*, Phys. Rev. D 64, 112007 (2001).
 [2] B. Armbruster *et al.*, Phys. Rev. D 65, 112001 (2002).
 [3] E. Church *et al.*, Phys. Rev. D 66, 013001 (2002).

- [4] B. T. Cleveland *et al.*, Astrophys. J. 496, 505 (1998).
 [5] J. N. Abdurashitov *et al.*, Phys. Rev. C 60, 055801 (1999).
 [6] W. Hampel *et al.*, Phys. Lett. B 447, 127 (1999).
 [7] S. Fukuda *et al.*, Phys. Lett. B 539, 179 (2002).
 [8] Q. R. Ahmad *et al.*, Phys. Rev. Lett. 87, 071301 (2001); Q. R. Ahmad *et al.*, Phys. Rev. Lett. 89, 011301 (2002); S. N. Ahmed *et al.*, Phys. Rev. Lett. 92, 181301 (2004).
 [9] K. Eguchi *et al.*, Phys. Rev. Lett. 90, 021802 (2003); T. Araki *et al.*, Phys. Rev. Lett. 94, 081801 (2005).
 [10] K. S. Hirata *et al.*, Phys. Lett. B 280, 146 (1992); Y. Fukuda *et al.*, Phys. Lett. B 335, 237 (1994).
 [11] Y. Fukuda *et al.*, Phys. Rev. Lett. 81, 1562 (1998).
 [12] W. W. M. Allison *et al.*, Phys. Lett. B 449, 137 (1999).
 [13] M. Ambrosio *et al.*, Phys. Lett. B 517, 59 (2001).
 [14] M. H. Ahn *et al.*, Phys. Rev. Lett. 90, 041801 (2003).
 [15] D. G. Michael *et al.*, Phys. Rev. Lett. 97, 191801 (2006).
 [16] M. Sorel, J. M. Conrad, and M. H. Shaevitz, Phys. Rev. D 70, 073004 (2004).
 [17] T. Katori, A. Kostelecky and R. Tayloe, Phys. Rev. D 74, 105009 (2006).
 [18] S. Kopp, Phys. Rept. 439, 101 (2007).
 [19] C. Athanassopoulos *et al.*, Nucl. Instrum. Meth. A388, 149 (1997).
 [20] S. Agostinelli *et al.*, Nucl. Instrum. Meth. A506, 250 (2003).
 [21] J. R. Sanford and C. L. Wang, Brookhaven National Laboratory, AGS internal reports 11299 and 11479 (1967) (unpublished).
 [22] M. G. Catanesi *et al.* [HARP Collaboration], arXiv:hep-ex/0702024; T. Abbott *et al.*, Phys. Rev. D45, 3906 (1992); J. V. Allaby *et al.*, CERN 70-12 (1970); D. Dekkers *et al.*, Phys. Rev. 137, B962 (1965); G. J. Marmar *et al.*, Phys. Rev. 179, 1294 (1969); T. Eichten *et al.*, Nucl. Phys. B44, 333 (1972); A. Aleshin *et al.*, ITEP-77-80 (1977); I. A. Vorontsov *et al.*, ITEP-88-11 (1988).
 [23] D. Casper, Nucl. Phys. Proc. Suppl. 112, 161 (2002).
 [24] A. Aguilar-Arevalo *et al.*, in preparation.
 [25] D. Ashery *et al.*, Phys. Rev. C 23, 2173 (1981).
 [26] H. Ejiri, Phys. Rev. C 48, 1442 (1993); F. Ajzenberg-Selove, Nucl. Phys. A506, 1 (1990); G. Garvey private communication.
 [27] D. Rein and L. M. Sehgal, Annals Phys. 133, 79 (1981).
 [28] CERN Program Library Long Writeup W5013 (1993).
 [29] B. C. Brown *et al.*, IEEE Nuclear Science Symposium Conference Record 1, 652 (2004).
 [30] D. Rein and L. M. Sehgal, Phys. Lett. B 104, 394 (1981).
 [31] T. Goldman, private communication.
 [32] B. Achkar *et al.*, Nucl. Phys. B434, 503 (1995).
 [33] B. P. Roe *et al.*, Nucl. Instrum. Meth. A543, 577 (2005); H. J. Yang, B. P. Roe, and J. Zhu, Nucl. Instrum. Meth. A555, 370 (2005); H. J. Yang, B. P. Roe, and J. Zhu, Nucl. Instrum. Meth. A574, 342 (2007).
 [34] Y. Liu and I. Stancu, arXiv:Physics/0611267 (to appear in Nucl. Instrum. Meth.).